Proceedings of the 25th International Conference on
Port and Ocean Engineering under Arctic Conditions
June 9-13, 2019, Delft, The Netherlands

Medium-scale Consolidation of Artificial Ice Ridge – Part II: Fracture Properties Investigation by a Splitting Test

Wenjun Lu[1], Aleksey Shestov[2], Sveinung Løset[1], Evgenii Salganik[1], Knut Høyland[1]
[1]Sustainable Arctic Marine and Coastal Technology (SAMCoT), Centre for Research-based Innovations (CRI), Norwegian University of Science and Technology, Trondheim, Norway
[2]The University Centre in Svalbard, Longyearbyen, Norway
[3]Delft University of Technology, Delft, Netherlands

ABSTRACT

Sea ice's fracture properties are in general difficult to measure and there is still on-going debate on the proper way to conduct valid measurements. Among many controversy fracture test conditions, the size of the test specimen and the loading rate were often raised. Given the circumstance, a series of large-scale sea ice's fracture tests were performed in Svalbard over the past few years from 2015 to 2018. As our test procedures get more matured and with existing test equipment, we performed a similar 'ice ridge splitting' test in 2017. The medium-scale ice ridge was prepared in February 2017; and in its course of consolidation, its associated morphological and mechanical properties (i.e., compressive strength in vertical and horizontal directions) were measured. At the end of this test, the ice ridge was split to introduce a global failure. In this ice ridge splitting experiment, we measured the splitting force history and the Crack Mouth Opening Displacement (CMOD) was derived according to Linear Elastic Fracture Mechanics (LEFM) theory. Aside from other physical and mechanical properties of this medium-scale ice ridge reported in the other associated paper, this paper (i.e., Part II of this series of papers) shall focus on its final fracture test and offer some insights into this ice ridge's fracture properties. Based on the calculation, we found the fracture energy of the artificial ice ridge is **12** J/m^2. This value is in a same level of those first-year sea ice's fracture energy measured in the field.

KEY WORDS: Fracture; Ice; Experiments; Fracture Energy; Ice Ridge

INTRODUCTION

Sea ice's fracture properties are in general difficult to measure and there is still on-going debate on the proper way to conduct valid measurements. Among many controversy fracture test conditions, the size of the test specimen and the loading rate were often raised. Given the circumstance, a series of large-scale sea ice's fracture tests were performed in Svalbard over the past few years from 2015 to 2018. The size of the fracture samples were chosen based on Linear Elastic Fracture Mechanics (LEFM) size requirements (Mulmule and Dempsey, 2000), namely, around 3 m. This size is larger than most, if not all, laboratory test samples (Dempsey, 1991). In addition, from 2015 to 2017, we have made consecutive upgrades to our loading system such that the loading rate was increasing from 0.015 mm/s, to 0.6 mm/s and then to 1.5 mm/s. With these efforts, the fracture tests were performed with a varying, but large enough sample size; and also, with a varying loading rate in a large range. Most of these tests were performed in the cut-free level ice samples. However, as our test procedures get more matured and with existing test equipment, we performed a similar 'ice ridge splitting' test in 2017. An artificial ice ridge was prepared in February 25th, 2017; and in its course of consolidation, its associated morphological and mechanical properties (i.e., compressive strength in vertical and horizontal directions) were measured. After around 42 days, on April 6th, 2017, the ice ridge was split to introduce a global failure. In this ice ridge splitting experiment, we measured the splitting force history and the Crack Mouth Opening Displacement (CMOD). Aside from other physical and mechanical properties of this medium-scale ice ridge reported in the other associated paper, this paper (i.e., Part II of this series of papers) shall focus on its final fracture test and offer some insights into this ice ridge's fracture properties.

METHOD

The idea behind the field fracture experiments, comparing to the laboratory fracture tests, is that the tested sample should be large enough to enclose a region, within which, all the nonlinear fracture activities take place. This region is the so-called Fracture Process Zone (FPZ). With LEFM theory, the size of this zone is 0. This means that all nonlinearities exist in this singular point and the stress there is infinite. Under this condition, a stress description of the material failure is no longer applicable and the concept of Stress Intensity Factor (SIF) and the fracture energy are introduced to cope with this infinite stress nuisance. This uncomfortable stress singularity issue was later modified and resolved by introducing a zone ahead of the crack tip. Within this zone, a stress profile that depends on the material property exists (Dugdale, 1960, Barenblatt, 1962). For quasi-brittle materials, such as concrete, rock and ice, the fictious crack model (Hillerborg et al., 1976) with a softening stress-separation curve to describe the failing material's properties within the FPZ is considered more general in characterizing the crack initiation and propagation for quasi-brittle material. As the size of the test sample becomes larger, this fictitious crack model reduces to the LEFM model. This model was first introduced into the ice research community by Mulmule and Dempsey (1998) and was later used to design and decode a series of large-scale ice fracture experiments (Dempsey et al., 1999a, Dempsey et al., 1999b).

In a series of studies (Lu et al., 2015b, Lu et al., 2015a), we reviewed the size requirement and loading rate requirements for such fracture tests. Combining practical issues, we end up with splitting an ice floe/ice ridge which is larger than 3 m with different loading rate. For the artificial ice ridge in this paper, it was split by a loading rate of 0.6 mm/s. The loading history was directly measured; together with the Crack Mouth Opening Displacement (CMOD) which can be derived. In a similar test, Dempsey et al. (2012) managed to split a 80 m-diameter ridged

multi-year ice floe and tried to estimate the fracture energy of the multi-year ice. In this paper, we shall take a similar approach and derive the fracture energy of the relatively better profiled artificial ice ridge's fracture energy. The approach basically follows the definition of fracture energy release rate G introduced by Irwin (1956) as in Eq. (1).

$$G = -\frac{d\prod}{dA} \tag{1}$$

$\prod$, defined in Eq.(2), is the potential energy of the elastic body and A is the area of the newly created crack.

$$\prod = U - WD \tag{2}$$

In Eq. (2), U is the strain energy stored in the body and WD is the work done by the external force. In our experiment, we are directly measuring the loading history whereas the CMOD at the loading area can be derived with certain confidence. This leads to the term WD in Eq. (2).

In this experiment, we are not monitoring the development of A. Instead, we take only two stages of the experiment into account. Namely, the initial stage with $\prod = 0, A = 0$ and the final stage with $\prod = -WD, A = A^*$. A^* is the area of the crack, which cuts the tested ridge into two. Comparing to the experiment carried out by Dempsey et al. (2012), we have a relatively better account for this value. This leads to the simplified calculation for fracture energy release rate as $G = WD / A^*$.

The fundamental assumption of using this method is that we have assumed the validity of LEFM in our experiment. The creeping effects, which later proves to be important, are excluded. However, considering the size of the test sample and the loading rate, this assumption is deemed as a 'not bad' assumption. In addition, during data processing (to be discussed), we deliberately exclude the non-relevant nonlinear behaviors (e.g., local creeping effects at the contact zone and the ice-structure contact building up process).

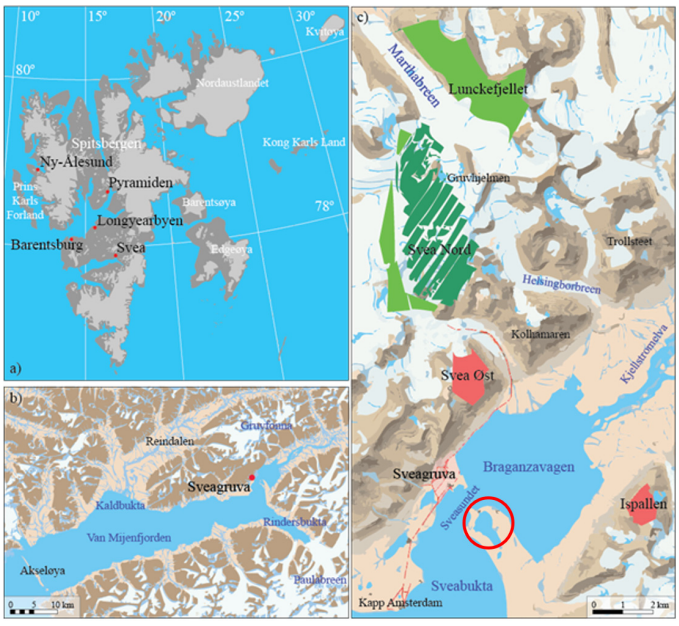

Figure 1. Overview of the chosen test field.

EXPERIMENT

Creation of the Ice Ridge

The chosen field is at the bay Braganzavågen in the Van Mijen Fjord of Spitsbergen (Figure 1a, b and c). The fjord is about 50 km long and spreads into Spitsbergen from the West to the East at about 77.8°N (Figure 1b). At the mouth, the fjord has width about 10 km, while to the head of the fjord it reduces to 5 km. There is the Akseløya island, at the mouth of the fjord, which blocks the fjord almost completely. This facilitates the process of stable land-fast ice formation. Water depth at the chosen test location is in a range of 5 to 10 meters.

The exact test location is within the Lake Vallunden in the Van Mijenfjorden in Svalbard (see the red circle in Figure 1c and see Figure 2 for a closer view). Lake Vallunden is a seawater lake connected with the seawater fjord by a small 100 m long channel (see Figure 2b). During the creation of the ice ridge, the level ice thickness is around 50 cm. To create the ice ridge, a trencher (see Figure 3a and with details described in Lu et al. (2015a)) was utilized to first cut a pool (5 m × 3 m) with a feeding channel (see Figure 3b). 55 ice blocks with sizes ranging between 80 cm × 42 cm × 50 cm to 134 cm × 43 cm × 50 cm were created and dumped randomly within the pool to form the initial stage of the artificial ice ridge (see Figure 3b). At the initial stage of the "ice ridge's" creation, it is merely a collection of loosely piled ice blocks without freeze bonds. The total ice volume is around 11.4 m^3. Moreover, the consolidated layer at this stage can be considered as 0 m thick.

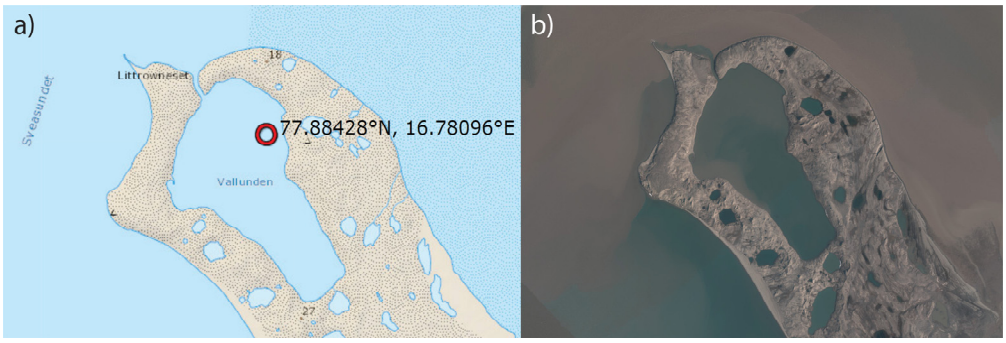

Figure 2. Exact test location of the artificial ice ridge splitting (left: exact location with GPS coordinate and right: satellite image during summer time showing the connectivity between the 'lake' and the surrounding sea water).

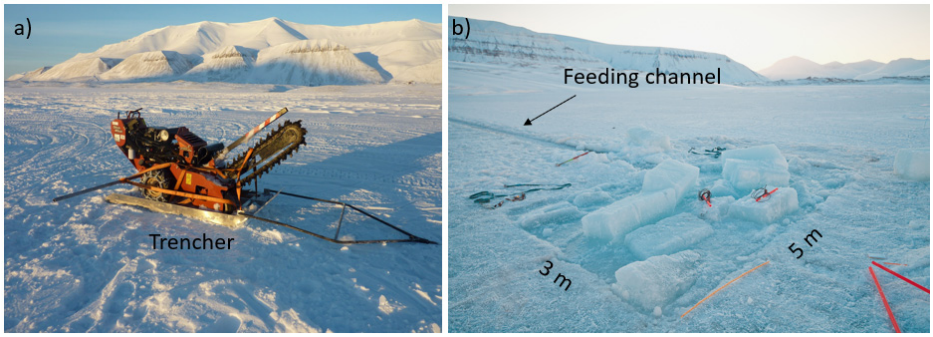

Figure 3. a) the trencher used to cut the ice blocks; b) initial stage of the created ice ridge (now is a collection of ice blocks not yet frozen together)

Splitting Test Preparation

After 42 days, according to measurements and calculations performed in the associated Paper I (Salganik et al., 2019), the ambient level ice thickness has been increased from 50 cm to 82 cm; and the consolidated layer has been increased from 0 cm to an average of 113 cm. An equally spaced 12-points profiling by drilling have been performed. Based on the ice ridge's vertical extends in these 12 points, the ice ridge's profile can be largely constructed. Figure 4 shows the re-constructed ice ridge's three-dimensional profile. The presented profile is not exactly the profile of the actual ice ridge. As the actual ice ridge has several protruded blocks included within (see e.g., Figure 3b). These abrupt changes cannot be captured by the 12-points' drilling data. Therefore, the re-constructed geometry in Figure 4 is only an approximate one instead of an accurate one. In order to perform the splitting experiment, the ice ridge was re-cut by the trencher along its borders until it becomes free-floating. Afterwards, a slot is cut (see Figure 5a) at the center of the ridge such that the loading device can be positioned there. Then, the initial crack is cut with the trencher to initiate the splitting crack at the center of the ridge (see Figure 5b).

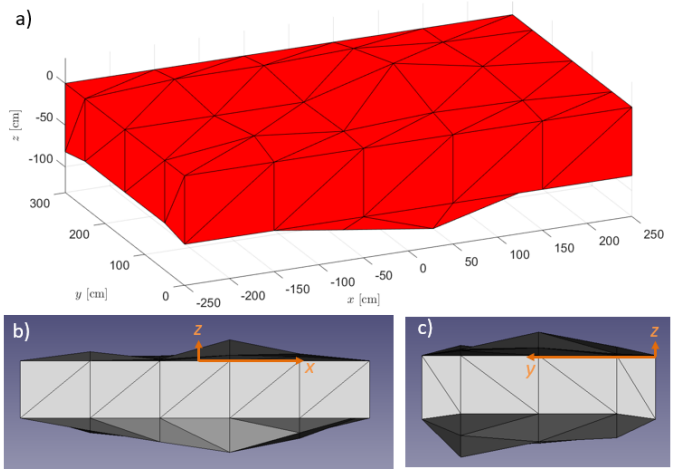

Figure 4. The re-constructed ice ridge's geometry based on 12 points' drilling data: a) perspective view with the chosen coordinate system and sizes; b) & c) side views.

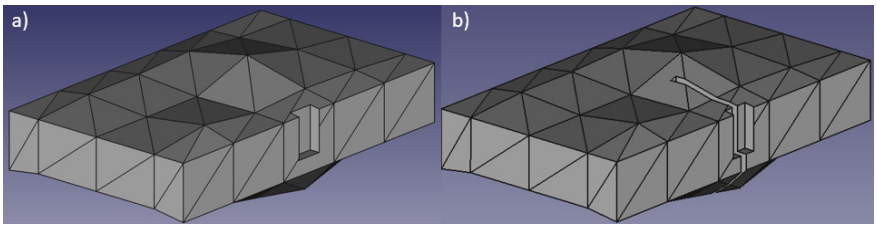

Figure 5. a) cutting the initial slots and b) initial crack for the splitting test.

After the ice ridge has been prepared, a purposely designed loading device is lowered and installed at the cut slot (see Figure 5a). The loading device has been fortified by adding pretensioned steel bars to make it as stiff as practically possible. The measured stiffness is around 50 kN/mm. Its major parameters and characteristics are illustrated in Figure 6. Moreover, the Jack is designed with a screw driving system, which enables constant displacement output. This creates a stable, displacement-controlled loading system in the fracture tests.

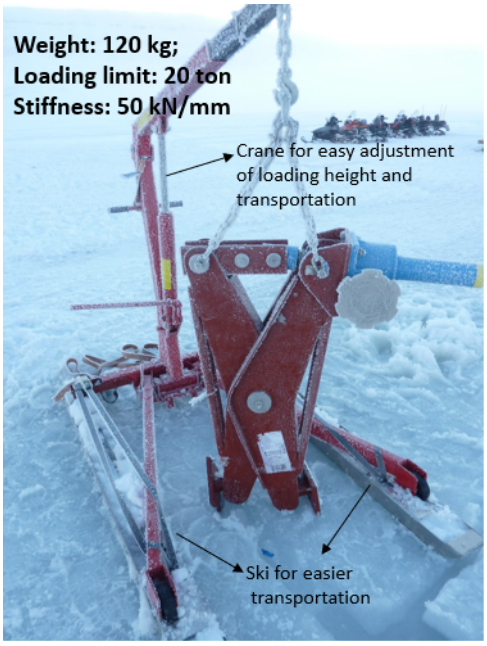

Figure 6. The screw-driven displacement-controlled loading device (i.e., the Jack).

Ice Ridge Splitting Test

Figure 7 shows the over view of ice ridge splitting test set-up and the morphology of the grown ice ridge after 42 days comparing to its initial stage in Figure 3b. According to both visual observation and drilled cores' integrity, most, if not all, the blocks were fully frozen within this artificial ridge and becomes a part of the consolidated layer.

Figure 7. Artificial ice ridge splitting test.

During the test, we utilized a constant output velocity of 0.6 mm/s to load the crack mouth area at the cut slot. At the same, a load cell that is installed within the Jack logs in the load history at a frequency of 1000 Hz.

Eventually, a crack starts from the manually cut 'crack tip' and propagates to the other side of

the ridge and splits the ice ridge into two. Along the crack path, several frozen blocks within the ice ridge has been obviously been 'cut through' by the crack. The crack did not propagate straight ahead but with a slight meandering before it reaches the other end of the ice ridge. With reference to Figure 4a & b, the crack propagates slightly to the left (i.e., $-x$ region) of the initial starting point at $x = 0$. This makes sense. As we can see from Figure 4b that a greater amount of ice mass exists to the right-hand side (i.e., $+x$ region) of the ice ridge, making the left hand side a relatively weaker zone preferred by the crack propagation.

Figure 8. After the ice ridge splitting test.

RESULTS AND DISCUSSIONS

The measured raw data of the loading history is presented in Figure 9. Several stages can be identified from the figure. Between the time segment a-b, the loading device's engine has been started and the jack is expanding at a rate of 0.6 mm/s. However, as there is no contact between the loading pad with the cut slot, no load was measured. Between segment b-c, there start to have some sort of contact which leads to the slight increase in the measure load. Between c-d, an increasingly stronger contact is built up between the loading pads and the ice sample. Presumably, local crushing at the contact area is taking place for the loading pad to bite into the ice sample and building a firmer contact. The loading curve in this range is rather nonlinear. Segment d-e features a sudden but relatively linear increase in the loading history. This segment lasts for 10.4 seconds (i.e., from Time = 132.2 s to 142.6s). Point e is the moment the initial crack starts to propagate and the measured load level decreases suddenly following the e-f curve (lasting for 7.4 s). Presumably, after point f, the final ligament area is broken off and the ridge is completely separated into two.

Given the loading history measured, it is of interest to select the region, within which, the Work Done (*WD*) by the external force can be related to the fracture energy. Aside the from the loading history, we also need to know the crack opening displacement history to calculate *WD*. Unfortunately, we have not measured the CMOD in this ice ridge splitting test due to practical difficulties on site. The surface of the ice ridge at the loading area is significantly uneven, due to the presence of frozen blocks. Therefore, we have to resolve to other means to estimate the crack opening displacement.

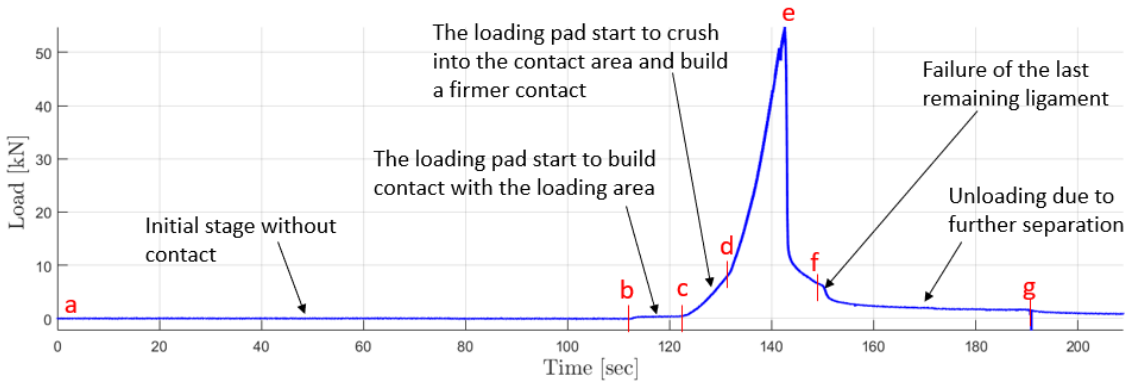

Figure 9. Raw measured load history during the ridge splitting test.

The first choice we had is rather straightforward. Since our experiment is displacement controlled, if the 0.6 mm/s expansion from the Jack is absolutely transferred to crack opening displacement, we can simply calculate the CMOD by multiplying the loading time by 0.6 mm/s. This also means that the Load – Displacement curve would behave as in Figure 10b with the selected region in Figure 10a, excluding the initial nonlinear contact building up processes.

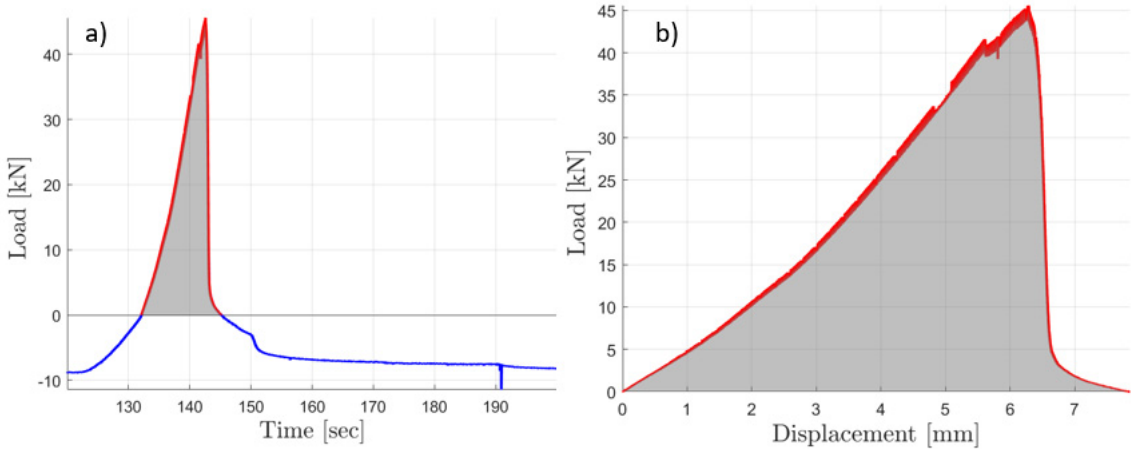

Figure 10. a) selected region to calculate the Work Done (*WD*) by external force; b) an incorrect way of deriving the displacement by simple multiplication.

However, the first choice we had is incorrect. With the shaded area in Figure 10b, we arrive at a significantly large *WD* = 138.16 J, which further leads to a 'fracture energy' of 71.15 J/m^2.

Therefore, we have to resolve to a relatively indirect approach to estimate the crack opening displacement. As mentioned previously, aside from this ridge splitting test, we have performed many other rectangular level ice's splitting tests. With the same loading rate, a typically measured loading history and Load-Displacement curve are shown in Figure 11a & b respectively.

Figure 11a shows that when the load starts to increase linearly (at around Time = 134.9 s) to its peak at around Time = 142.6 s, it takes around 7.7 s. Using the previously direct approach, this would be translated into a displacement of 7.7 s × 0.6 mm/s = 4.62 mm at the load peak. However, as reflected from Figure 11b, the CMOD reaches only 0.824 mm at the load peak; and before the load increases to, e.g., 4 kN, there is little CMOD increase. So, an obvious question is, where goes the Jack's 4.62 mm expansion in this process as we see only 0.824 mm CMOD reaches on ice? One explanation to this would be due to the presence of local creep at

the contact area. Even though the loading rate is rather high, our test experience tells that ice creeps instantly as loaded. This local creeping effect dissipates a large amount of the Jack's expansion and transfer only a small portion (around 1/6) of the displacement to the entire sample. This part of the energy dissipation should be excluded from our calculation of *WD*. Aside from the tested level ice sample shown in Figure 11, other similar tested samples also show that the ice fails at a peak CMOD of around 0.8 mm.

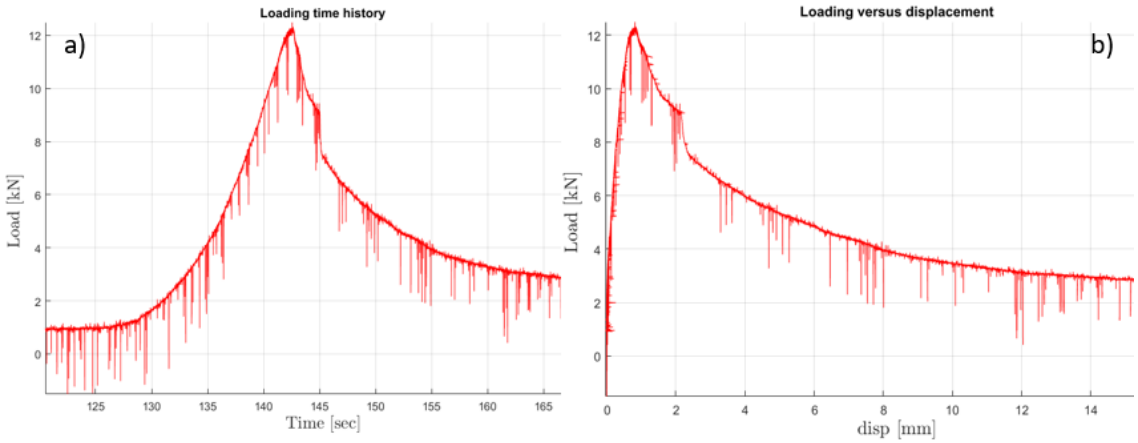

Figure 11. A typical level ice (size: 5 m × 10 m; initial crack length 3 m) floe's splitting test with a loading rate of 0.6 mm/s.

According to the fictious crack model, the traction-separation curve is a material property. This means that the maximum separation should be same for the same ice irrespective of its geometry. Given this statement, we further assume that we can indirectly scale the CMOD history tested on a level ice floe to the ice ridge. Recall that the normalized crack opening profile $u(a,0)$ can be written in Eq. (3), in which,

$$u(a,0)=\frac{U(a,0)}{L}=\frac{P}{tLE'}\int_0^a h_r^2(s,0)ds \tag{3}$$

$U(a,0)$ is the half crack opening displacement at different initial crack location a.

P is the applied load level.

t is the ice thickness. For the level ice tested in Figure 11, $t=0.6\,\text{m}$, whereas the average ice ridge's thickness is about 1.13 m.

E' $E'=E$ for a plane stress condition, and $E'=E/(1-v^2)$ for a plane strain condition (where E is Young's modulus and v is the Poisson ratio).

$h_r(s,0)$ is the normalized weight function for an Edge Cracked Rectangular Plate (ECRP). This function can be found in Dempsey and Mu (2014).

In these two tests (see Figure 9 and Figure 11), we can assume that E' are the same. The remaining corresponding CMOD $U(a,0)$ scaling is left with the term of P/t and $\int_0^a h_r^2(s,0)ds$. The dimensionless term $\int_0^a h_r^2(s,0)ds$ is plotted in Figure 12 showing the variation of half-crack profile along the initial crack length. In our case, we are mainly

interested in the scaling of CMOD at the center of the loading area for the tested level ice and ice ridge with an initial crack length of $a = 0.6$ and $a = 0.4$, respectively. Given the related parameters presented in Eq. (3), the scaled maximum CMOD for the ice ridge test is found to be 1.053 mm, according to Tables 1 to 3 and Eq. (4).

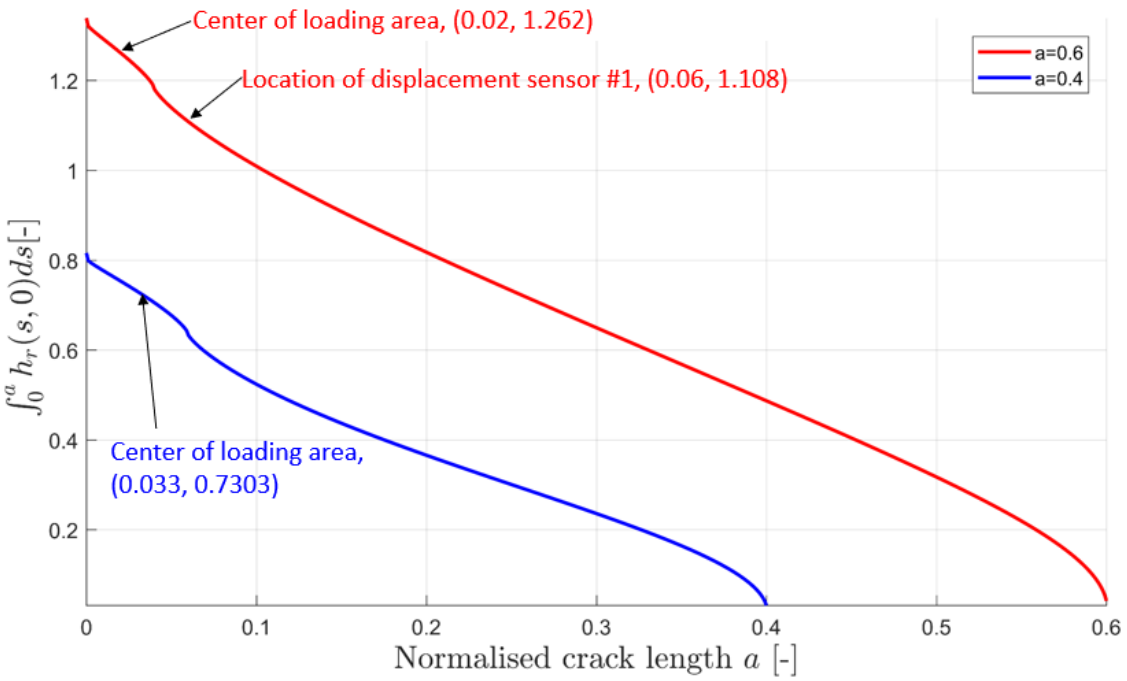

Figure 12. Scaling of crack profile with initial crack length.

Table 1. Scaling of P/t for the two different tests.

	a	L	t	P	P/t
Level ice floe	0.6	5 m	0.6 m	12.49 kN	20.82 kN/m
Ice ridge	0.4	3 m	1.13 m	45.60 kN	40.35 kN/m

Table 2. Scaling of nondimensionalized displacement $\int_0^a h_r^2(s,0)ds$ for the two different tests.

$\int_0^a h_r^2(s,0)ds$	at displacement sensor #1	at center of loading area
Level ice floe	1.108	1.262
Ice ridge	-	0.7303

Table 3. Scaling of maximum CMOD $2U(a,0)$ for the two different tests.

CMOD $2U(a,0)$	at disp sensor #1	at center of loading area
Level ice floe	0.824 mm (measured)	0.939 mm (scaled according to Figure 12)
Ice ridge	-	**1.053 mm** (calculated according Eq. (4))

$$\frac{2U^R(a=0.4,0)}{2U^L(a=0.6,0)} = \frac{P^R/t^R}{P^L/t^L}\frac{\int_0^{a=0.4} h_r^2(s,0)ds}{\int_0^{a=0.6} h_r^2(s,0)ds}$$

$$2U^R(a=0.4,0) = \frac{P^R/t^R}{P^L/t^L}\frac{\int_0^{a=0.4} h_r^2(s,0)ds}{\int_0^{a=0.6} h_r^2(s,0)ds}2U^L(a=0.6,0) \quad (4)$$

$$= \frac{40.35\,\text{kN/m}}{20.82\,\text{kN/m}} \cdot \frac{0.7303}{1.262} \cdot 0.939\,\text{mm}$$

$$= 1.053\,\text{mm}$$

Eq. (4) shows in detail how the CMOD 1.053 mm for the ice ridge test is scaled. The upper script 'R' and 'L' in Eq. (4) represent corresponding values for the ice ridge test and level ice test respectively.

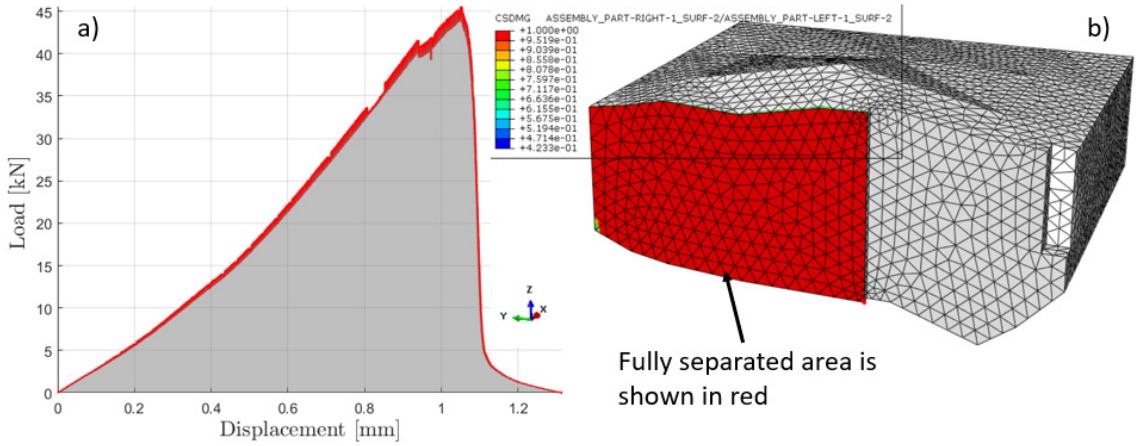

Figure 13. a) Load-Displacement curve with scaled displacement (i.e., maximum displacement at load peak is 1.053 mm); b) right-hand-side of the ice ridge with separated areas (in red) simulated by Abaqus.

With the calculated maximum crack opening displacement of 1.053 mm for the ice ridge test, we can further scale the Load-Displacement curve in Figure 10b to the following Figure 13a. The shaded area in Figure 13a leads to a value of WD = 23.15 J. This value is much less comparing to the one derived by simple multiplication (i.e., 138.16 J). The area of the cracked surface (i.e., illustrated in Figure 13b) is A^* = 1.94 m^2, with which, the energy release rate is calculated as G = **12** J/m^2 for the tested artificial ice ridge.

The energy release value is obviously larger than those measured from the lab (i.e., around 1 J/m^2); however, in a same level of those back calculated from the field tests of first year sea ice (i.e., 10 ~ 15 J/m^2 (Dempsey et al., 2018)).

The greatest uncertainty involved in the calculation of this paper is the derivation of CMOD by scaling a similar splitting test from a nearby level ice floe. The scaling is purely based on LEFM theory. Given the tested sample size and relatively faster loading rate, the applicability the LEFM theory is considered trustworthy in this case. Using the LEFM theory, we manage to get rid of a tremendous amount of local creeping displacement; around 89% of the Jack's expansion displacement goes into the local creeping displacement. With the relatively linear

Load-Displacement curve's shaded area, we end up with the value of 8.17 J/m^2. This value should be considered as a lower value because certain amount of elastic strain energy might be stored during the local creeping process, which was radically excluded in our calculation in selecting the shaded area in Figure 10a.

CONCLUSIONS

An artificial ice ridge was created in February 2017. After 42 days of natural consolidation, the ice ridge was split by purposely designed device, i.e., the Jack. Thanks to a screw-driven system, is loading device is capable of output a displacement-controlled loading process. During the test, the ice ridge was loaded at the crack mouth with a constant speed of 0.6 mm/s until its failure. In this process, the loading history was logged. Because of the relatively large size of the ice ridge and fast loading speed, we assumed the applicability of Linear Elastic Fracture Mechanics (LEFM) theory in analyzing the test data. By scaling the Crack Mouth Opening Displacement (CMOD) of a nearby level ice's splitting test, we found that there is a large amount of local creep displacement (around 89% of the Jack's output displacement) at the contact area. With the derived CMOD for the ridge splitting, we calculated a fracture energy of 12 J/m^2 for the created artificial ice ridge. This value is in a same level of those tested in the field by Dempsey et al. (2018). Given the uncertainties involved in deriving the CMOD for the ice ridge splitting and the simplified calculation based on LEFM, further study on other test data are needed. In those level ice floe's splitting tests, more thorough measurements were performed, and thus more reliable results can be obtained.

ACKNOWLEDGEMENTS

The authors would like to thank the Norwegian Research Council through the research center of SAMCoT CRI for financial support in carrying out the experiment. The first author would also like to thank VISTA – a basic research program in collaboration between The Norwegian Academy of Science and Letters, and Equinor (former Statoil), for financial support in writing this paper.

REFERENCES

BARENBLATT, G. I. 1962. The mathematical theory of equilibrium cracks in brittle fracture. *Advances in applied mechanics,* 7**,** 55-129.

DEMPSEY, J., COLE, D., WANG, S. & SCIENCES, E. 2018. Tensile fracture of a single crack in first-year sea ice. *Journal of Philosophical Transactions of the Royal Society A: Mathematical, Physical,* 376**,** 20170346.

DEMPSEY, J. P. 1991. The fracture toughness of ice. *Ice-Structure Interaction***,** 109–145.

DEMPSEY, J. P., ADAMSON, R. M. & MULMULE, S. V. 1999a. Scale effects on the in-situ tensile strength and fracture of ice. Part II: First-year sea ice at Resolute, NWT. *International journal of fracture,* 95**,** 347-366.

DEMPSEY, J. P., DEFRANCO, S. J., ADAMSON, R. M. & MULMULE, S. V. 1999b. Scale effects on the in-situ tensile strength and fracture of ice Part I: Large grained freshwater ice at Spray Lakes Reservoir, Alberta. *International journal of fracture,* 95**,** 325-345.

DEMPSEY, J. P. & MU, Z. 2014. Weight function for an edge-cracked rectangular plate. *Engineering Fracture Mechanics,* 132**,** 93-103.

DEMPSEY, J. P., XIE, Y., ADAMSON, R. M. & FARMER, D. M. 2012. Fracture of a ridged multi-year Arctic sea ice floe. *Cold Regions Science and Technology,* 76–77**,** 63-68.

DUGDALE, D. S. 1960. Yielding of steel sheets containing slits. *Journal of the Mechanics and Physics of Solids,* 8**,** 100-104.

HILLERBORG, A., MODEER, M. & PETERSSON, P. E. 1976. Analysis of crack formation and crack growth in concrete by means of fracture mechanics and finite elements. *Cement and concrete research,* 6**,** 773-781.

IRWIN, G. R. Onset of fast crack propagation in High Strength Steel and Aluminum Alloys. Sagamore Research Conference Proceedings, 1956. 289-305.

LU, W., LØSET, S., SHESTOVE, A. & LUBBAD, R. Design of a field test for measuring the fracture toughness of sea ice. *In:* KIM, E., LU, W. & HØYLAND, K., eds. The 23rd International Conference on Port and Ocean Engineering under Arctic Conditions, June 14-18, 2015 2015a Trondheim, Norway.

LU, W., LUBBAD, R. & LØSET, S. 2015b. In-plane fracture of an ice floe: A theoretical study on the splitting failure mode. *Cold Regions Science and Technology,* 110**,** 77-101.

MULMULE, S. V. & DEMPSEY, J. P. 1998. A viscoelastic fictitious crack model for the fracture of sea ice. *Mechanics of Time-dependent Materials,* 1**,** 331-356.

MULMULE, S. V. & DEMPSEY, J. P. 2000. LEFM size requirements for the fracture testing of sea ice. *International journal of fracture,* 102**,** 85-98.

SALGANIK, E., HØYLAND, K., SHESTOV, A., LØSET, S. & HEIJKOOP, A.-N. 2019. Medium-scale consolidation of artificial ice ridge – Part I: surface temperature, thickness and mechanical properties. *Proceedings of the 25th International Conference on Port and Ocean Engineering under Arctic Conditions.* Delft, The Netherlands.